

## The JLab 12GeV Upgrade and the Initial Science Program

VOLKER D. BURKERT

*Jefferson Lab, Newport News, VA 23606, USA*

*Lecture given at the International School of Physics 'Enrico Fermi', 2011, Varenna, Italy*

**Summary.** — An overview is presented of the upgrade of JLab's cw electron accelerator from a maximum beam energy of currently 6 GeV to 12 GeV. Construction of the upgrade project has started in 2008. A broad experimental program has been developed to map the nucleon's intrinsic correlated spin and momentum distribution through measurements of deeply exclusive and semi-inclusive processes, and to probe the quark and gluon confinement by studying the spectrum of mesons with exotic quantum numbers. Other programs include the forward parton distribution function at large  $x_B$ , the quark and gluon polarized distribution functions, the measurements of electromagnetic form factors of the nucleon ground state and of nucleon resonance transitions at high  $Q^2$ , and the exploration of physics beyond the Standard Model in high precision parity violating processes. The 12 GeV electron beam is also well suited to explore quark hadronization properties using the nucleus as a laboratory.

PACS 13.60.-r, 13.60.Hb, 13.60.Fz, 13.60.Le, 13.40.Gp, 14.20.Gk - .

## Table of Content

Page	Section
2	1. Introduction
4	2. The Electron Accelerator and the 12 GeV Experimental Equipment.
6	3. Generalized Parton Distributions and DVCS
10	4. Semi-inclusive DIS and TMDs
13	5. Inclusive structure functions and moments
14	5'1. Valence quark structure and flavor dependence at large $x$ .
15	5'2. Spin structure functions and parton distributions
15	5'3. Global analysis of polarized parton densities
15	5'4. Moments of spin structure functions
18	6. Elastic and resonance transition electromagnetic form factors at short distances
18	6'1. Nucleon elastic form factors
18	6'2. Nucleon resonance transition form factors
18	7. Gluonic Hadron spectroscopy.
18	7'1. Hybrid mesons
22	7'2. Hybrid baryons
23	8. Quarks and hadrons in the nuclear medium
23	8'1. Color Transparency
23	8'2. Quark propagation and hadron formation.
23	9. Search for new Physics
23	9'1. Search for deviations from the Standard Model
25	9'2. Heavy photon search
27	10. Conclusions
27	References

## 1. – Introduction

The challenge of understanding nucleon electromagnetic structure still continues after more than five decades of experimental scrutiny. From the initial measurements of elastic form factors to the accurate determination of parton distributions through deep inelastic scattering (DIS), the experiments have increased in statistical and systematic accuracy. It was realized in recent years that the parton distribution functions represent special cases of a more general, and much more powerful way of characterizing the structure of the nucleon, the generalized parton distributions (GPDs) [1, 2, 3, 4, 5]. The GPDs describe the simultaneous distribution of particles with respect to both position and momentum. In addition to the information about the spatial density (form factors) and momentum density (parton distribution), these functions reveal the correlation of the spatial and momentum distributions, *i.e.* how the spatial shape of the nucleon changes when probing quarks of different wavelengths.

The concept of GPDs has led to completely new methods of “spatial imaging” of the nucleon, either in the form of two-dimensional tomographic images, or in the form of genuine three-dimensional images. GPDs also allow us to quantify how the orbital motion of quarks in the nucleon contributes to the nucleon spin – a question of crucial importance for our understanding of the “dynamics” underlying nucleon structure. The spatial view of the nucleon enabled by the GPDs provides us with new ways to test dynamical models of nucleon structure. The mapping

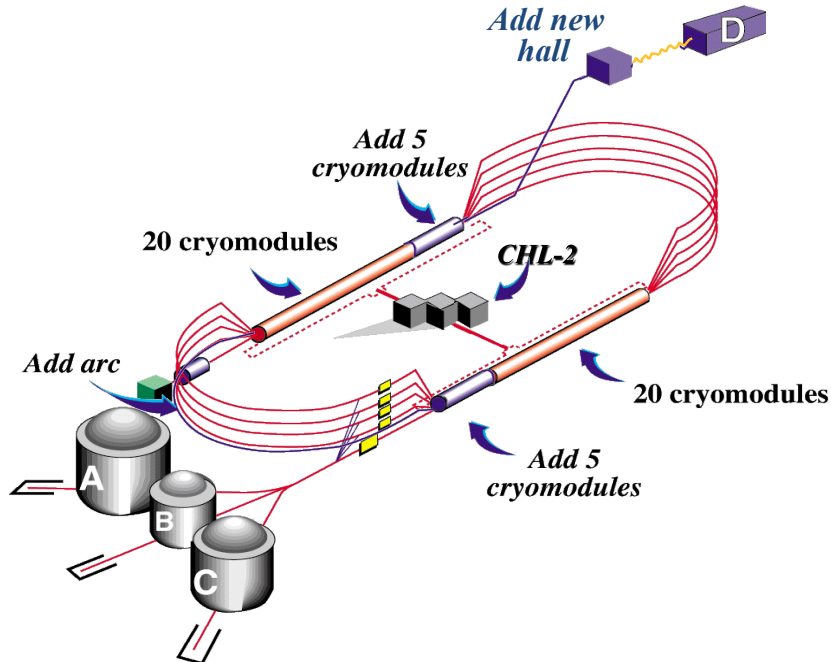


Fig. 1. – The Jefferson Lab continuous electron beam accelerator facility showing the components needed for the 12 GeV upgrade.

of the nucleon GPDs, and a detailed understanding of the spatial quark and gluon structure of the nucleon, have been widely recognized as the key objectives of nuclear physics of the next decade. This requires a comprehensive program, combining results of measurements of a variety of processes in electron–nucleon scattering with structural information obtained from theoretical studies, as well as with expected results from future lattice QCD simulations.

While GPDs, and also the more recently introduced transverse momentum dependent distribution functions (TMDs), open up new avenues of research, the traditional means of studying the nucleon structure through electromagnetic elastic and transition form factors, and through flavor- and spin-dependent parton distributions must also be employed with high precision to extract physics on the nucleon structure in the transition from the regime of quark confinement to the domain of asymptotic freedom. These avenues of research can be explored using the 12 GeV cw beam of the JLab upgrade with much higher precision than has been achieved before, and can help reveal some of the remaining secrets of QCD. Also, the high luminosity available will allow us to explore the regime of extreme quark momentum, where a single quark carries 80% or more of the proton’s total momentum.

The strong force is mediated by the exchange of gluons between quarks as well as between gluons. Their presence has been observed in high energy scattering experiments where they generate a third jet of particles in addition to the 2 jets coming from the fragmentation of the scattered quarks. A clear understanding of the role of gluons in interactions at the lower energies is still missing. Models that describe the interaction through gluon flux tubes predict that the glue plays an active role and can be excited and lead to novel states of mesons and baryons. The search of some of these hybrid states is the focus of the photo production

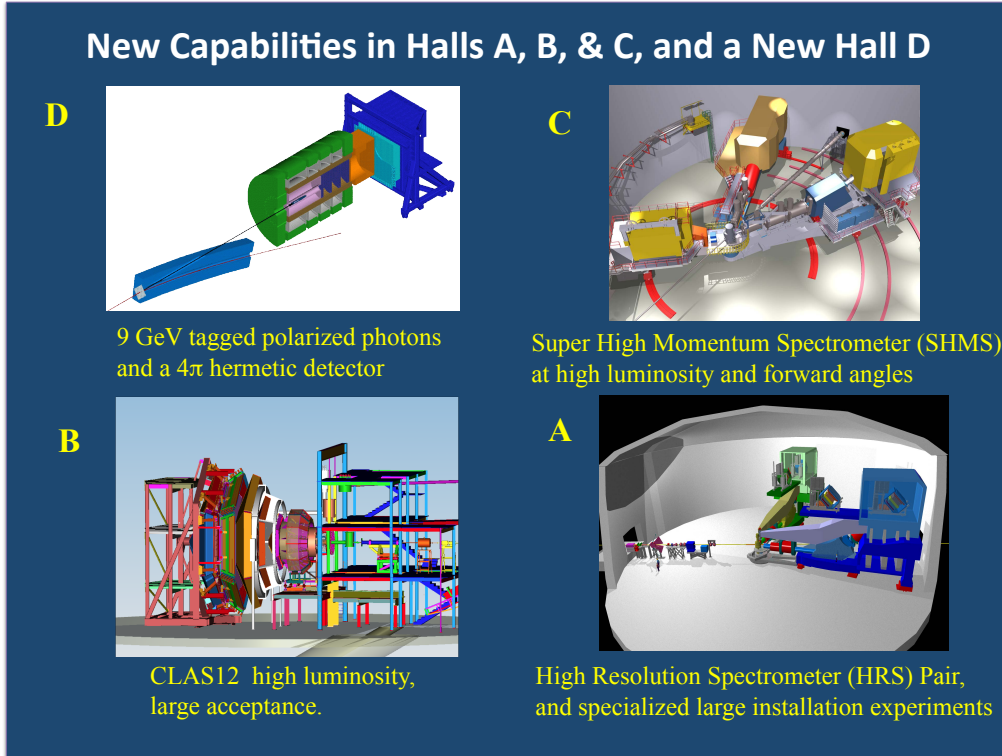


Fig. 2. – Baseline experimental equipment to support the scientific program for the JLab 12 GeV energy upgrade Description in the text.

experiments in the new Hall D. The plan for this report is to give a brief overview in section 2 of the upgrade of the JLab accelerator to 12 GeV and briefly discuss the experimental equipment that is currently under construction to carry out the science program during the first 5 years of operation. In section 3 and section 4 I discuss the program to study the generalized parton distribution function (GPDs) and the transverse momentum dependent functions (TMDs) using polarization degrees-of-freedom, which covers a major part of this contribution and are the main ingredients to develop the multi-dimensional representation of quarks in the nucleon in coordinate and momentum space. In sections 7 through 9, I discuss some of the other programs: spectroscopy, form factors and structure functions at high  $Q^2$ , nuclear processes, and physics beyond the SM. Since this is an overview covering a broad future physics program, I will not be able to go into depth of any of the topics discussed. The phenomenological underpinnings of much of the material, especially the part related to GPDs and TMDs, has been presented in lectures and seminars in the earlier part of the school by experts, and I refer the reader to these contributions for details in this volume.

## 2. – The Electron Accelerator and the 12 GeV Experimental Equipment.

The electron accelerator is shown schematically in Fig. 1. The two linear accelerators are based on superconducting rf technology. Spin polarized electrons are generated in the gun and pre-

TABLE I. – Sensitivity of deeply virtual Compton scattering and deeply virtual meson production processes to the leading twist GPDs for different quark flavors.

	Process	Flavor	$q/\bar{q}/g$	
$\mathcal{H}, \mathcal{E}, \tilde{\mathcal{H}}, \tilde{\mathcal{E}}$	pDVCS	$4u + d + s$	$q + \bar{q}, \alpha_S g$	
	nDVCS	$4d + u + s$	$q + \bar{q}, \alpha_S g$	(polarized) deuteron
$\mathcal{H}, \mathcal{E}$	$\rho^+$	$u - d$	$q + \bar{q}, g$	$\text{Im}(\mathcal{H}E^*)$ in $A_{UT}$
	$\rho^0$	$2u + d$	$q + \bar{q}, g$	
	$\omega$	$2u - d$	$q + \bar{q}, g$	
	$\phi$	$s$	$q + \bar{q}, g$	
	$J/\psi, \Upsilon$		$g$	
	$(\pi^+ \pi^-)_{L=0}$	$2u - d$	$q - \bar{q}$	interfere with $(\pi^+ \pi^-)_{L=1}$
	$K^{*0} \Sigma^+, K^{*+} \Sigma^0$	$d - s$	$2q - \bar{q}$	SU(3)
	$K^{*+} \Lambda$	$2u - d - s$	$2q - \bar{q}$	SU(3)
$\tilde{\mathcal{H}}, \tilde{\mathcal{E}}$	$\pi^+$	$\Delta u - \Delta d$	$2q - \bar{q}$	
	$\pi^0$	$2\Delta u + \Delta d$	$q - \bar{q}$	
	$\eta$	$2\Delta u - \Delta d + 2\Delta s$	$q - \bar{q}$	
	$K^{*0} \Sigma^+, K^{*+} \Sigma^0$	$d - s$	$2q + \bar{q}$	SU(3)
	$K^{*+} \Lambda$	$2u - d - s$	$2q + \bar{q}$	SU(3)

accelerated to 50MeV in the injector shown at the upper left end of the racetrack. They are then boosted in the north linac to about 600 MeV. They are then bent by 180 degrees and injected into the south linac to be accelerated to up to 1200 MeV. This is repeated four more times when the final energy of 6000 MeV is reached. For the energy upgrade five accelerating cryo-modules with four times higher gradients per unit length are added to both linacs to reach a maximum energy at the existing end stations of nearly 11 GeV. One arc and one more path through the north linac are added to accelerate the beam to 12 GeV and transport it to the new Hall D. Major equipment upgrades are planned to support a broad program of nuclear physics, hadron spectroscopy, and the exploration of the quark-gluon dynamics and multi-dimensional structure of the nucleon. The base equipment that is part of the 12GeV upgrade scope is under construction and is scheduled for completion in the fall of 2014. The base equipment in the four Halls is shown in Fig. 2. The focus in Hall D is on the study of hybrid mesons with exotic quantum numbers to understand the excitation of the glue in hadronic systems. Hall D houses a large hermitic detector that is based on a solenoid magnet, and has tracking capabilities and photon detection over nearly the full  $4\pi$  solid angle. The bottom left panel shows the new CLAS12 large acceptance spectrometer, with large angular coverage and increased luminosity. The top panel on the right shows the spectrometer pair of forward focusing spectrometers in Hall C including the new SHMS spectrometer on the left. In Hall A the existing HRS2 spectrometer pair will be retained. In addition, the Hall will house large installation equipment for specialized experiments. The solenoid detector in Hall

D, CLAS12 and the SHMS are part of the base equipment, and are projected to be available for physics by the end of 2014. There are additional pieces of equipment proposed that are outside the scope of the 12GeV project and require separate funding. In Hall A several proposals are under consideration, a super gig bite spectrometer (SBS) with large solid angle, a spectrometer (Moller) to measure parity violation in electron-electron scattering, and a solenoid detector for parity violation experiments in DIS and for SIDIS experiments (SOLID). There are also efforts underway to incorporate a large acceptance RICH detector into CLAS12 for improved charged particle identification capabilities, and various ancillary detectors for neutron detection and quasi-real photon tagging. Complementing the new equipment that is under construction, are the highly polarized electron gun, high power cryogenic targets, and several polarized targets using  $\text{NH}_3$ ,  $\text{ND}_3$ , HD, butanol, and  $^3\text{He}$  to support a broad range of polarization measurements.

### 3. – Generalized Parton Distributions and DVCS

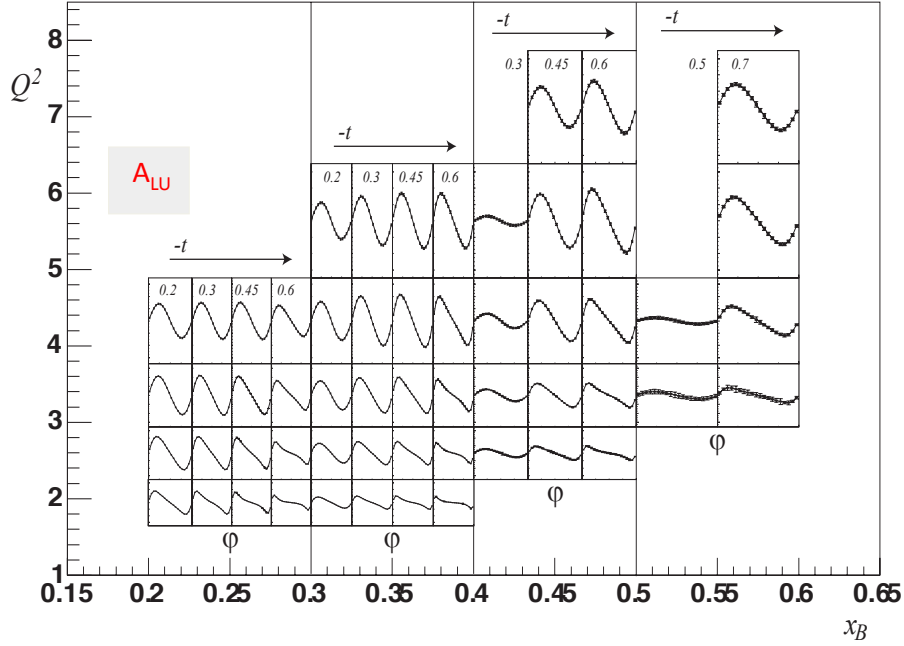


Fig. 3. – Projected data for the azimuthal dependence of the beam spin asymmetry  $A_{LU}$  for experiment [15].

It is now well recognized [2, 6, 7, 8] that deeply virtual Compton scattering and deeply virtual meson production are most suitable for mapping out the twist-2 vector GPDs  $H$ ,  $E$  and the axial GPDs  $\tilde{H}$ ,  $\tilde{E}$  in  $x$ ,  $\xi$ ,  $t$ , where  $x$  is the momentum fraction of the struck quark,  $\xi$  the longitudinal momentum transfer to the quark, and  $t$  the transverse momentum transfer to the nucleon. Having access to a 3-dimensional image of the nucleon (two dimensions in transverse space, one dimension in longitudinal momentum) opens up completely new insights into the complex internal structure and dynamics of the nucleon. In addition, GPDs carry information

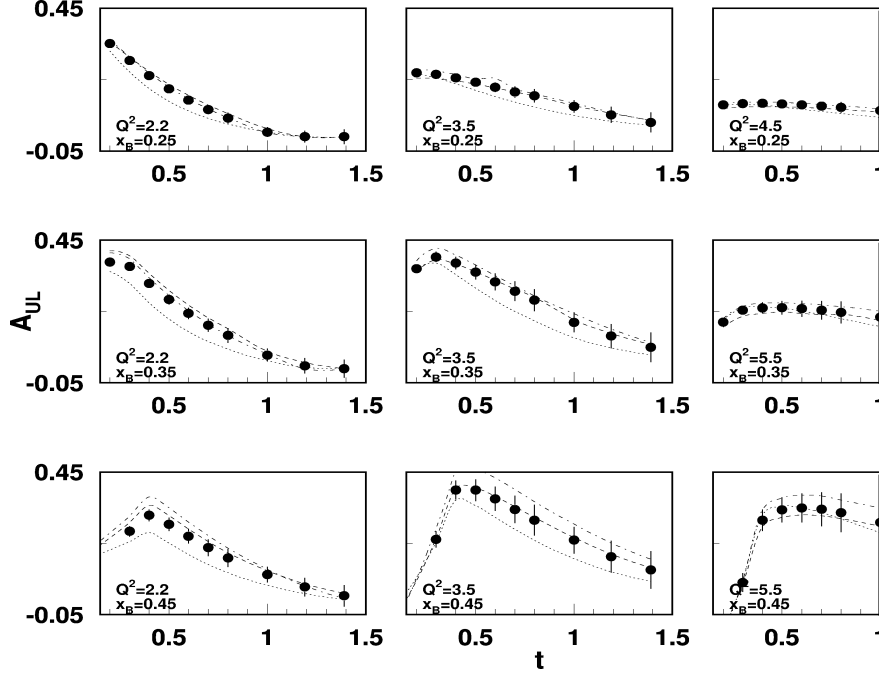


Fig. 4. – Projected data for the  $t$ -dependence of the longitudinal target spin asymmetry  $A_{UL}$  for experiment [15].

of more global nature. For example, the nucleon matrix element of the energy-momentum tensor contains 3 form factors that encode information on the angular momentum distribution  $J^q(t)$  of the quarks with flavor  $q$  in transverse space, their mass-energy distribution  $M_2^q(t)$ , and their pressure and force distribution  $d_1^q(t)$ . How can we access these form factors? The only known process to directly measure them is elastic graviton scattering off the nucleon. However, these form factors also appear as moments of the two vector GPDs [9], thus offering prospects of accessing gravitational form factors through the detailed mapping of GPDs. The quark angular momentum form factor in the nucleon is given by

$$J^q(t) = \int_{-1}^{+1} dx x [H^q(x, \xi, t) + E^q(x, \xi, t)] ,$$

and the mass-energy and pressure distribution

$$M_2^q(t) + 4/5 d_1^q(t) \xi^2 = \int_{-1}^{+1} dx x H^q(x, \xi, t) .$$

The mass-energy and force-pressure distribution of the quarks are given by the second moment of GPD  $H$ , and their relative contribution is controlled by  $\xi$ . A separation of  $M_2^q(t)$  and  $d_1^q(t)$  requires measurement of these moments in a large range of  $\xi$ . The beam helicity-dependent cross section asymmetry is given in leading twist as

$$A_{LU} \approx \sin \phi [F_1(t)H + \xi(F_1 + F_2)\tilde{H}]d\phi ,$$

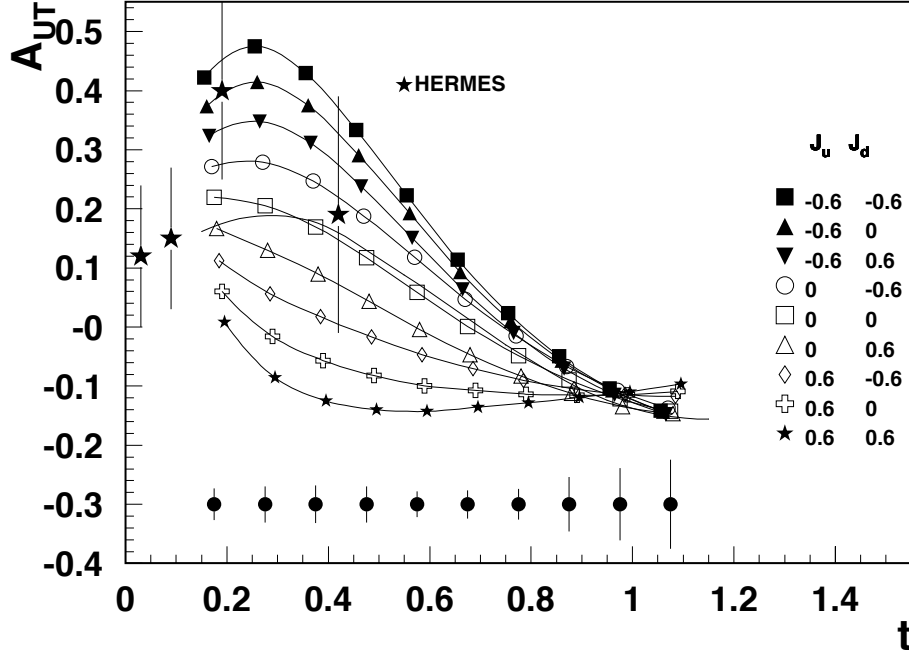


Fig. 5. – Projected data for the  $t$ -dependence of the transverse target spin asymmetry  $A_{UT}^{\sin \phi \cos \phi - \phi_s}$ . The  $t$  dependence of  $A_{UT}$  is shown for a single bin at  $Q^2 = 2\text{GeV}^2$  and  $x=0.25$  [16].

where  $\phi$  is the azimuthal angle between the electron scattering plane and the hadronic production plane. The kinematically suppressed term with GPD  $E$  is omitted. The asymmetry is mostly sensitive to the GPD  $H(x = \xi, \xi, t)$ . In a wide kinematics [10, 11] the beam asymmetry  $A_{LU}$  was measured at Jefferson Lab at modestly high  $Q^2$ ,  $\xi$ , and  $t$ , and in a more limited kinematics [12] the cross section difference  $\Delta\sigma_{LU}$  was measured with high statistics. Moreover, a first measurement of the target asymmetry  $A_{UL} = \Delta\sigma_{UL}/2\sigma$  was carried out [13], where

$$A_{UL} \approx \sin \phi [F_1 \tilde{H} + \xi(F_1 + F_2)H] .$$

The combination of  $A_{LU}$  and  $A_{UL}$  allows the separation of GPD  $H(x = \xi, \xi, t)$  and  $\tilde{H}(x = \xi, \xi, t)$ . Using a transversely polarized target the asymmetry

$$A_{UT} \approx \cos \phi \sin(\phi - \phi_s) [t/4M^2(F_2H - F_1E)]$$

can be measured, where  $\phi_s$  is the azimuthal angle of the target polarization vector relative to the electron scattering plane.  $A_{UT}$  depends in leading order on GPD  $E$ . Measurement of  $A_{UT}$  may thus be the most efficient way of determining GPD  $E$ .

First DVCS experiments carried out at JLab [10, 11, 12, 13] and DESY [14] showed promising results in terms of the applicability of the handbag mechanism to probe GPDs. The 12 GeV

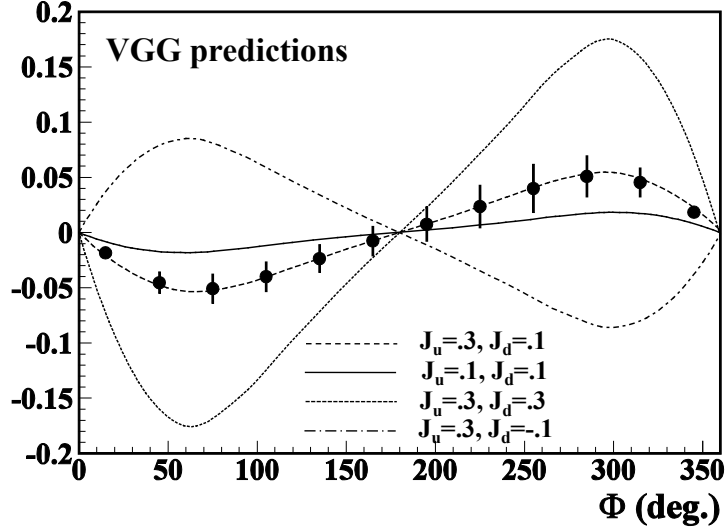


Fig. 6. – Projections of experiment [19] for the DVCS beam-spin asymmetry  $A_{LU}$  on the neutron for one bin in  $Q^2$ ,  $x_B$ ,  $t$ . The different lines indicate expected asymmetries for different values of the nucleon spin carried by  $u$  and  $d$  quarks as predicted by the VGG model [20]. The magnitude of  $A_{UL}$  on the neutron is predicted much smaller than what has been measured on the proton.

upgrade offers much improved possibilities for accessing GPDs. Figure 3 shows the expected statistical precision of the DVCS-BH beam asymmetry for some sample kinematics. Using a longitudinally polarized target one can also measure the target spin asymmetries  $A_{UL}$  with high precision. Figure 4 shows the expected statistical accuracy for the moment  $A_{UL}^{sin\phi}$ . Using a transversely polarized target, the transverse target spin asymmetry  $A_{UT}$  can be measured. The  $t$ -dependence of  $A_{UT}$  as projected in [16] is shown in Fig. 5 for a single bin in  $Q^2$  and  $x$ .

Measurements of all 3 asymmetries will allow a separate determination of GPDs  $H$ ,  $\tilde{H}$  and  $E$  at the above specified kinematics. If the  $t$ -dependences are known, a Fourier transformation of GPD  $E(x = \xi, t)$  can be used to determine the polarized quark distribution in transverse impact parameter space. To obtain a complete picture of the quark distribution in the nucleon, the GPDs need to be measured for both flavors  $u$ -quarks and  $d$ -quarks. This requires measurement of DVCS not only on the proton but also on the neutron. Experiment [19] will measure the beam-spin asymmetry for the neutron  $en(p_s) \rightarrow e\gamma n(p_s)$

Figure 7 shows simulated images of the quark distributions in transverse space using a model parameterization of GPDs [7].

Deeply virtual exclusive meson production (pseudo scalar mesons and vector mesons) will play an important role in disentangling the flavor- and spin-dependence of GPDs (see table I). For exclusive mesons only the longitudinal photon coupling in  $\gamma^*p \rightarrow Nm$  enables direct access to GPDs through the handbag mechanism and must be isolated from the transverse coupling. That the transverse contribution cannot be neglected at currently available energies of 6 GeV was observed in the non-zero beam asymmetry measured with CLAS [17] that indicated the presence of a significant longitudinal-transverse interference term in the amplitudes. In addition, the dominance of the handbag mechanism in the longitudinal cross section must first be established

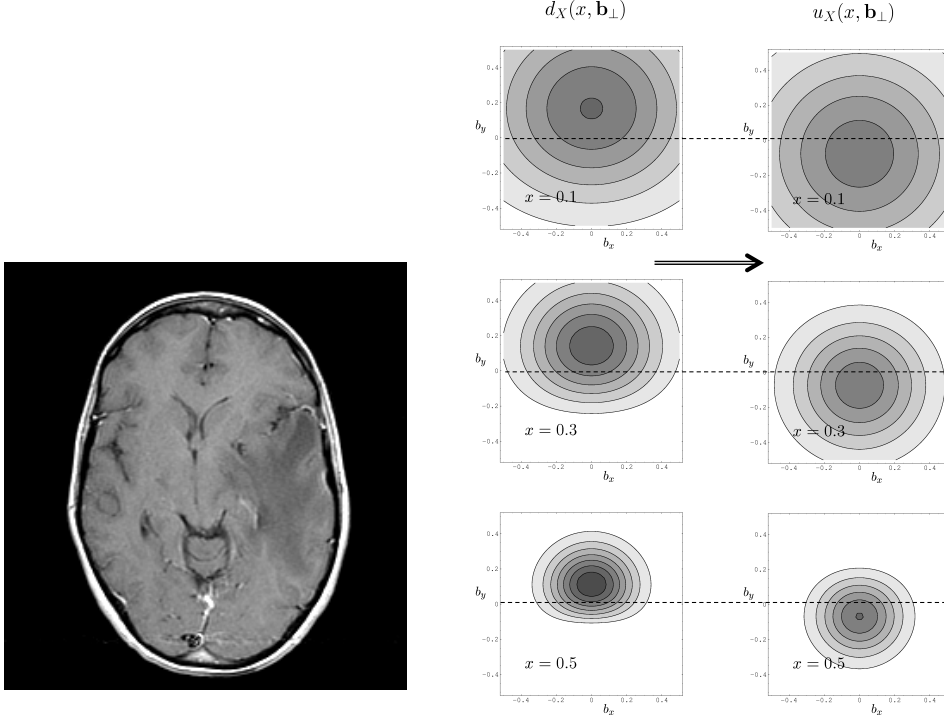


Fig. 7. – Left panel: Slice of a 3-D tomographic image of a human brain from an CAT scan. Right panel: Simulated quark distributions in a transversely polarized proton. The arrow indicates the direction of the polarization. The centroids of the d-quarks (left column) appear shifted upwards and the distributions appear deformed from the symmetric distribution in unpolarized protons; the centroids of the u-quark distributions are shifted in the opposite direction, generating a  $u-d$  quark flavor dipole.

at the upgrade energy before meson production may be incorporated in a global fit of all hadronic reactions to extract GPDs.

#### 4. – Semi-inclusive DIS and TMDs

Semi-inclusive deeply inelastic scattering (SIDIS) processes, where the leading, high momentum hadron is detected in coincidence with the scattered lepton, are used for “flavor tagging” of quarks to select contributions from different quark species. Currently, the emphasis is to study SIDIS processes that encode information on the transverse momentum distributions of quarks, information that is not otherwise accessible. For example, azimuthal distributions of final state particles in SIDIS provide access to the orbital motion of quarks and play an important role in the study of transverse-momentum dependent distributions (TMDs) of quarks in the nucleon.

TMD distributions describe transitions of a nucleon with one polarization in the initial state to a quark with another polarization in the final state. The diagonal elements in the table II

TABLE II. – *Leading-twist transverse momentum-dependent distribution functions. U, L, and T stand for transitions of unpolarized, longitudinally polarized, and transversely polarized nucleons (rows) to corresponding quarks (columns).*

N/q	U	L	T
U	$\mathbf{f}_1$		$h_1^\perp$
L		$\mathbf{g}_1$	$h_{1L}^\perp$
T	$f_{1T}^\perp$	$g_{1T}$	$\mathbf{h}_1$ $h_{1T}^\perp$

are the momentum, longitudinal and transverse spin distributions of partons, and represent well-known parton distribution functions related to the square of the leading-twist, light-cone wave functions. Off-diagonal elements require non-zero orbital angular momentum and are related to the wave function overlap of  $L=0$  and  $L=1$  Fock states of the nucleon. The chiral-even distributions  $f_{1T}^\perp$  and  $g_{1T}$  are the imaginary parts of the corresponding interference terms, and the chiral-odd  $h_1^\perp$  and  $h_{1L}^\perp$  are the real parts. The TMDs  $f_{1T}^\perp$  and  $h_1^\perp$  are related to the imaginary part of the interference of wave functions for different orbital momentum states and

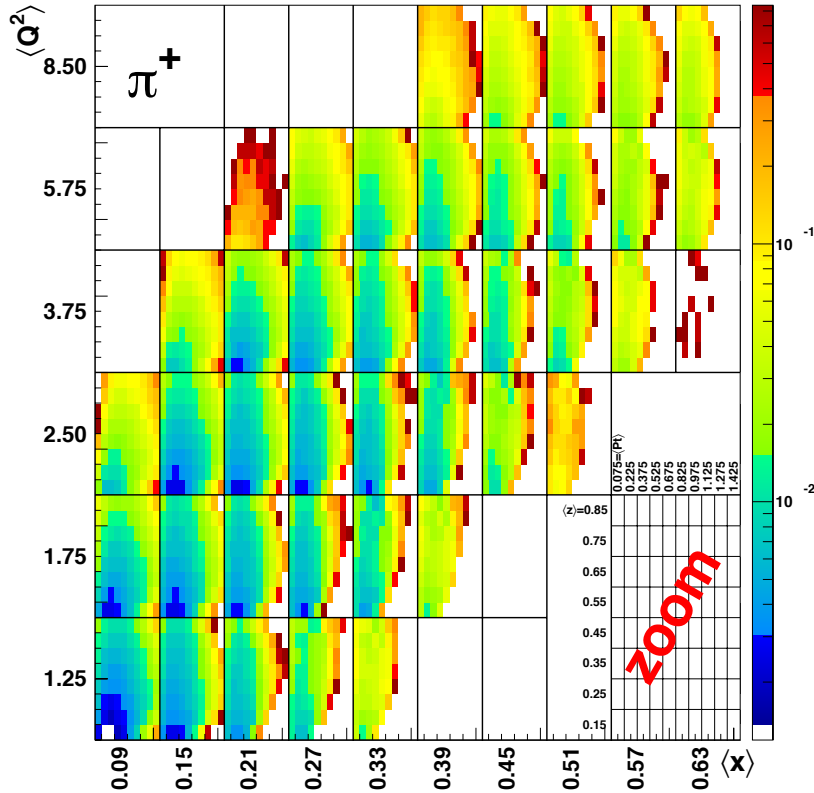


Fig. 8. – Kinematic coverage and projected uncertainties of the 4-dimensional  $\pi^+$  yield in  $Q^2$ ,  $x$ ,  $z$ , and  $p_T$ . The color code shows the relative errors in each bin.

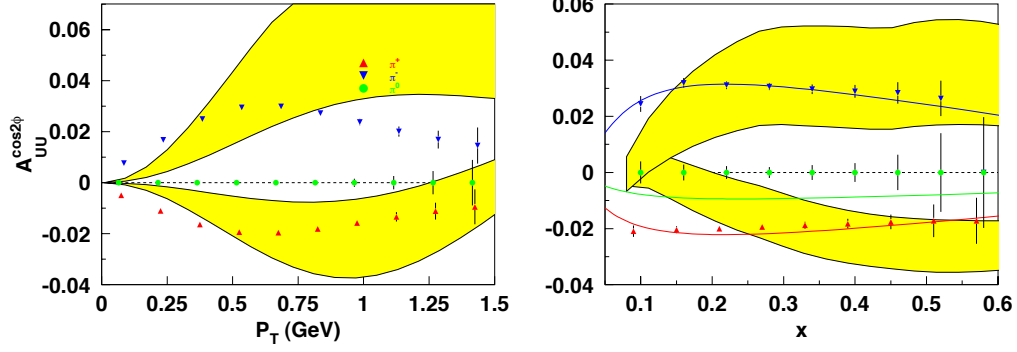


Fig. 9. – The  $\cos 2\phi$  moment (Boer-Mulders asymmetry) for pions as a function of  $Q^2$  and  $P_T$  for  $Q^2 > 2 \text{ GeV}^2$  with CLAS12 at 11 GeV from 2000 hours of running. Values are calculated assuming  $H_1^{\perp u \rightarrow \pi^+} = -H_1^{\perp u \rightarrow \pi^-}$ . Only statistical uncertainties are shown. The yellow band between the two curves indicates the range of two model predictions.

are known as the Sivers [21] and Boer-Mulders [22, 23] functions. They describe unpolarized quarks in the transversely polarized nucleon and transversely polarized quarks in the unpolarized nucleon, respectively. The most simple mechanism that can lead to a Boer-Mulders function is a correlation between the spin of the quarks and their orbital angular momentum. In combination with a final state interaction that is on average attractive, already a measurement of the sign of the Boer-Mulders function, would thus reveal the correlation between orbital angular momentum and spin of the quarks.

Similar to the extraction of GPDs, TMD studies will greatly benefit from the higher energy

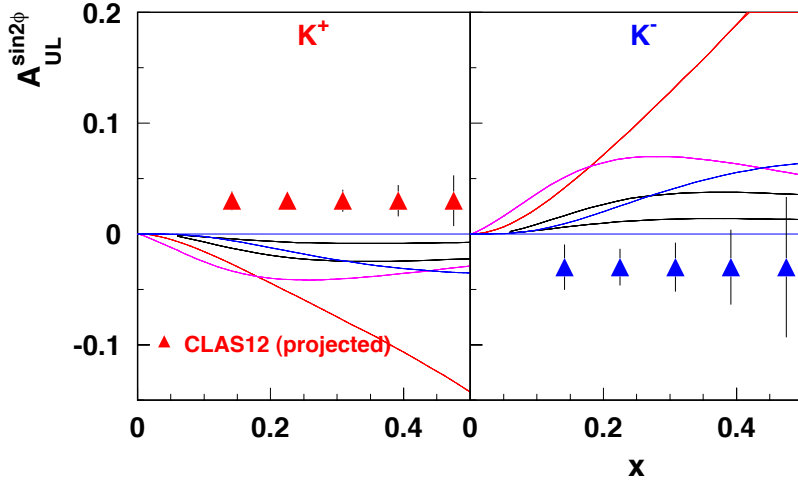


Fig. 10. – Projected  $x$ -dependence of the polarized spin target asymmetry at 11 GeV with CLAS12 for kaons for one bin in  $Q^2$ ,  $z$ ,  $p_T$ .

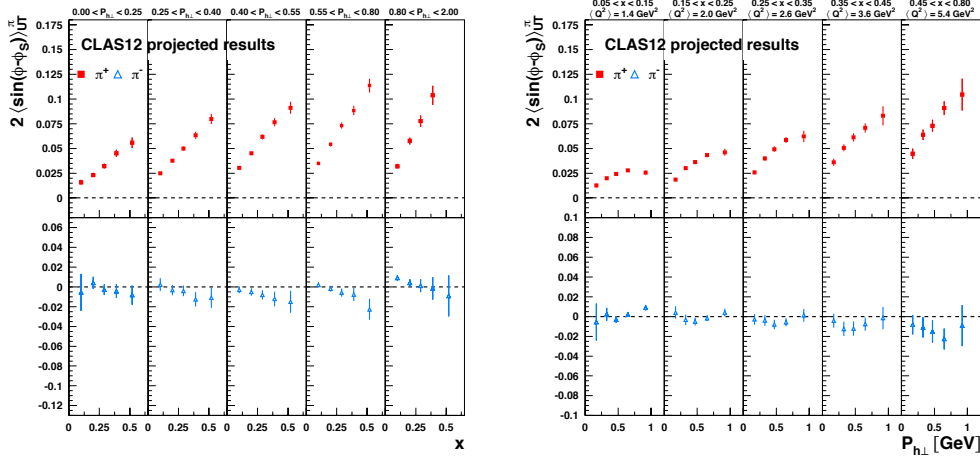


Fig. 11. – Projected data for the Siverts function vs  $x$  for different transverse momentum bins (left panel) and vs  $p_T$  for different  $x$  bins.

and luminosity available at 12 GeV. A comprehensive program is in preparation at JLab to study the new quark distribution functions. The main focus is on the measurement of SIDIS processes in the full 4-D phase space available in  $Q^2$ ,  $x$ ,  $z$  and  $p_T$ . Fig. 8 shows the phase space coverage and statistical precision expected for semi-inclusive  $\pi^+$  production proposed in [29]. Examples of kinematics coverage and statistical accuracy are presented in Fig. 9.

Several experiments will measure the Mulders-Kotzinian asymmetry on longitudinally polarized proton target [29, 30] and on  $^3\text{He}$  target [31]. Figure 10 shows an example of the expected asymmetry and statistical precision for charged kaon production. Several experiments have been proposed to study the Siverts asymmetries on polarized  $^3\text{He}$  [33] and on polarized hydrogen [34, 35]. Examples of kinematic dependences are shown in Fig. 11. Although pions have been the main focus of SIDIS experiment in the past, the  $K^+$  and  $K^-$  channels have recently emerged as of high interest as well. Hermes results show unexpectedly large Boer-Mulders asymmetries for kaons compared to pions, and the opposite signs for  $K^-$  and  $\pi^-$ . Several experiments [25, 26, 28, 30, 34] will measure semi-inclusive processes for kaon productions. With the excellent particle identification and high luminosity expected for CLAS12, these puzzling issues can be addressed efficiently. Figure 10 shows the statistical precision for  $K^+$  and  $K^-$  production on longitudinally polarized hydrogen in one kinematic bin in  $Q^2$ ,  $z$ , and  $p_T$ .

The experimental effort will produce high quality asymmetry data in a large range of the 4-dimensional space of  $Q^2$ ,  $x$ ,  $z$ ,  $p_T$ . The challenge will be to extract from these large amounts of data the TMDs that encode the quark's intrinsic spin-momentum correlations.

## 5. – Inclusive structure functions and moments

Polarized and unpolarized structure functions of the nucleon offer a unique window into the internal quark longitudinal momentum and helicity densities of nucleons. The study of these structure functions provides insight into the two defining features of QCD — asymptotic freedom at small distances, and confinement and non-perturbative effects at large distance scales. After more than three decades of measurements at many accelerator facilities worldwide, a truly impressive amount of data has been collected, covering several orders of magnitude in both kinematic variables  $x$  and  $Q^2$ . However, there are still important regions of the accessible phase

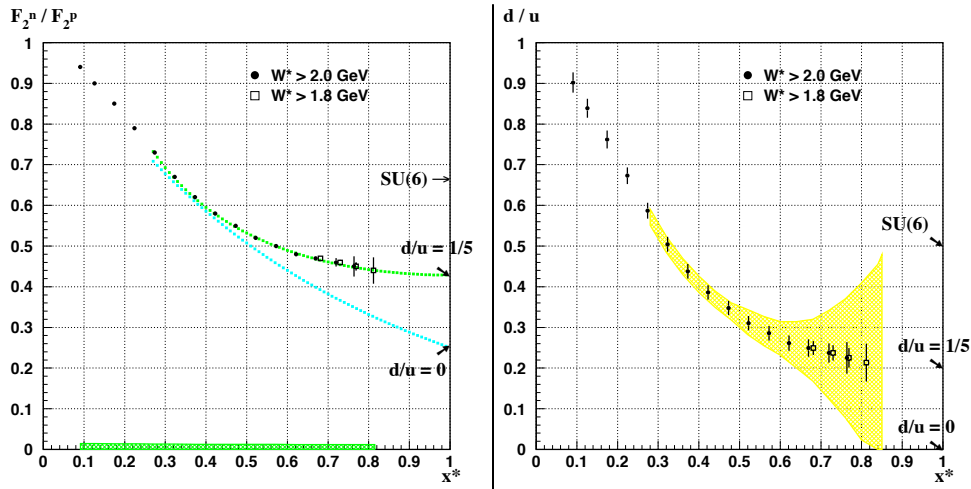


Fig. 12. – Projected data for the ratio  $F_2^n/F_2^p$  (left) and  $d/u$  (right) for 11 GeV beam energy [41]. The error bars in the right panel contain both statistical and systematic uncertainties. The yellow area shows the uncertainty of current data due to poorly known nuclear corrections.

space where data are scarce and have large uncertainties, and where significant improvements are possible through precise experiments at Jefferson Lab.

One of the open questions is the behavior of the structure functions in the extreme kinematic limit  $x \rightarrow 1$ .

In this region effects from the virtual sea of quark-antiquark pairs are suppressed, making this region simpler to model than the small  $x$  region. This is also the region where pQCD can make absolute predictions. However, the large  $x$  domain is difficult to reach as cross sections are kinematically suppressed, the parton distributions are small and final states interactions (partonic or hadronic) are large. First steps into the large  $x$  domain became possible at energies of 5-6 GeV [51, 37]. The interest triggered by these first results and the clear necessity to extend the program to larger  $x$  (for recent reviews see: [39, 40]) provided one of the cornerstone of the JLab 12 GeV upgrade physics program.

**5.1. Valence quark structure and flavor dependence at large  $x$ .** – The unpolarized proton structure function  $F_2^p(x)$  has been mapped out in a large range of  $x$  leading to precise knowledge of the quark distribution  $u(x)$ . The corresponding structure function  $F_2^n(x)$  is well measured only for  $x < 0.5$  as nuclear corrections, using deuterium as a target, are large and very uncertain at  $x > 0.5$ . Corrections for Fermi motion are clearly insufficient. At JLab, a new technique tested recently has been shown very effective in reducing the nuclear corrections. The results of the BONUS experiment have recently been published [38]. The experiment uses a novel radial time-projection-chamber (rTPC) with gas-electron-multiplier (GEM) readout as detector for the low-energy spectator proton in the reaction  $en(p_s) \rightarrow ep_s X$ . Measurement of the spectator proton for momenta as low as 70 MeV/c and at large angles minimizes the poorly known nuclear corrections at large  $x$ . The techniques will be used with CLAS12 to accurately determine the ratio  $d(x)/u(x)$  to much larger  $x$  values [41]. Figure 12 shows the projected data for  $F_2^n(x)/F_2^p(x)$  and  $d(x)/u(x)$ . A dramatic improvement is projected at large  $x$ . Another experiment in Hall A [42] measures inclusive scattering on two mirror nuclei  ${}^3\text{He}$  and  ${}^3\text{H}$  for which the nuclear wave functions are very similar. The cross section ratio  $\sigma(e {}^3\text{He} \rightarrow e X)/\sigma(e {}^3\text{H} \rightarrow e X)$  is then largely free of nuclear corrections and the ratio of structure functions  $F_2^n/F_2^p$  can be extracted.

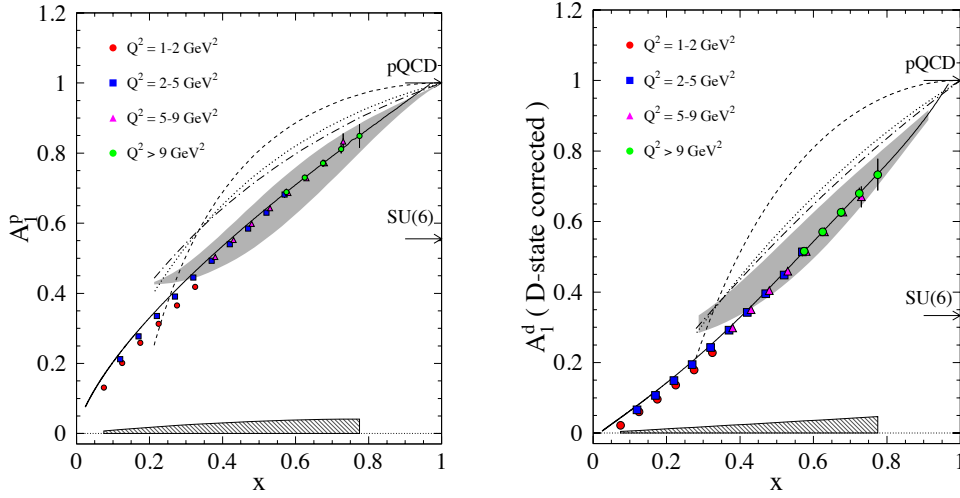


Fig. 13. – Anticipated results on  $A_1^p$ . The four different symbols represent four different  $Q^2$  ranges. The statistical uncertainty is given by the error bars while the systematic uncertainty is given by the shaded band.

**5.2. Spin structure functions and parton distributions.** – The lack of precise data in the valence quark region and especially at very large  $x$  values is even more obvious for the spin structure function  $g_1(x, Q^2)$ , both on the proton and neutron. New experiments at 12 GeV will significantly improve our knowledge of the basic spin structure function. Two experiments will study polarized parton distributions at  $x \leq 0.9$  on polarized protons and polarized neutrons. Using standard detection equipment, a redesigned polarized target adapted to CLAS12 and 30 (50) days of running [43] on a longitudinally polarized  $\text{NH}_3$  ( $\text{ND}_3$ ) target, high precision results can be achieved as shown in Fig. 13. Similar coverage is projected using a polarized  ${}^3\text{He}$  as a quasi-neutron target in Hall A [44]. These data will discriminate among models in the large- $x$  region. The projected results shown in Fig. 13 are with a  $W > 2$  GeV constraint. Studies of hadron-parton duality will tell us if this constraint can be relaxed so that spin structure functions may be used for  $x \leq 0.9$  in the extraction of parton spin densities from global fits including these data. Results on protons and neutrons targets will allow for the extraction of the d-quark polarization  $(\Delta d + \Delta \bar{d})/(d + \bar{d})$ , and the asymmetry of the polarized sea  $x[\Delta \bar{u}(x) - \Delta \bar{d}(x)]$ . The accuracy expected from these measurements is shown in Fig. 14.

**5.3. Global analysis of polarized parton densities.** – The larger window that will open up over the DIS domain with the 12 GeV upgrade will permit more stringent constraints of the parton distributions in global fits to polarized structure functions. JLab data at lower energies had already unique impact at large  $x$ . The improvement from the 12-GeV upgrade is also significant at low and moderate  $x$ , noticeably for the polarized gluon distribution  $\Delta G$ . To demonstrate the precision achievable with the expected CLAS12 data, we have plotted in Fig. 15 the expected impact of future JLab data at 12 GeV on the next-to-leading order QCD analyses of the polarized gluon distribution [46]. A dramatic improvement can be achieved with the expected data from experiment E12-06-109 [43]. The data will not only reduce the error band on  $\Delta G$ , but will likely allow a more detailed modeling of its  $x$ -dependence. Significant improvements are expected for the quark distributions as well, especially for the polarized  $s$  quark density.

**5.4. Moments of spin structure functions.** – Moments of structure functions are related to the nucleon static properties by sum rules. Inclusive deep inelastic scattering data at JLab

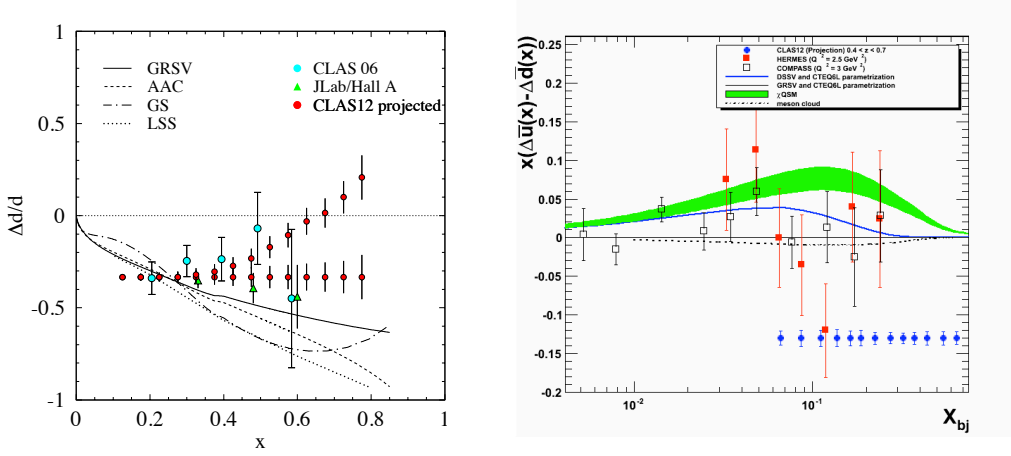


Fig. 14. – Left panel: Expected results for  $(\Delta d + \Delta \bar{d})/(d + \bar{d})$ . The central values of the data are following two arbitrary curves to demonstrate how the two categories of predictions, namely the ones that predict  $\Delta d/d$  stays negative (LO and NLO analyses of polarized DIS data: GRSV, LSS, AAC, GS, statistical model, and a quark-hadron duality scenario) and the ones predicting  $\Delta d/d \rightarrow 1$  when  $x \rightarrow 1$  (leading order pQCD and a quark-hadron duality scenario). The right panel shows the expected uncertainties for the asymmetry of the polarized sea quarks.

have permitted evaluation of the moments at low and intermediate  $Q^2$  [47, 48, 49, 51, 50]. With a maximum beam energy of 6 GeV, however, the measured fractional strength of the moments becomes rather limited for  $Q^2$  greater than a few  $\text{GeV}^2$ . The 12-GeV upgrade extends this range to much higher  $Q^2$ . At sufficiently large  $Q^2$ , the Bjorken sum rule relates the integral  $\Gamma_1^{p-n} = \int (g_1^p - g_1^n) dx$  to the nucleon axial charge [52]. Figure 16 shows the expected precision on  $\Gamma_1^p$ . Published results and preliminary results from CLAS are also displayed for comparison. The hatched blue band corresponds to the systematic uncertainty on the CLAS EG1b data points. The red band indicates the estimated systematic uncertainty from CLAS12. The systematic uncertainties for EG1 and CLAS12 include the estimated uncertainty on the unmeasured DIS part estimated using a frequently used model [53]. As can be seen, moments can be measured up to  $Q^2=6 \text{ GeV}^2$  with a statistical accuracy improved several fold over that of the existing world data.

Finally, moments in the low ( $\simeq 0.5 \text{ GeV}^2$ ) to moderate ( $\simeq 4 \text{ GeV}^2$ )  $Q^2$  range enable us to extract higher-twist parameters, which represent correlations between quarks in the nucleon. This extraction can be done by studying the  $Q^2$  evolution of the first moments [54, 60]. Higher twists have been consistently found to have, overall, a surprisingly smaller effect than expected. Going to lower  $Q^2$  enhances the higher-twist effects but makes it harder to disentangle a high twist from the yet higher ones. Furthermore, the uncertainty on  $\alpha_s$  becomes prohibitive at low  $Q^2$ . Hence, higher twists turn out to be hard to measure, even at the present JLab energies. Adding data at higher  $Q^2$  to the present JLab data set removes the issues of disentangling higher twists from each other and of the  $\alpha_s$  uncertainty. The smallness of higher twists, however, requires statistically precise measurements with small point-to-point correlated systematic uncertainties. Such precision at moderate  $Q^2$  has not been achieved by the experiments done at high energy accelerators, while JLab at 12 GeV presents the opportunity to reach it considering the expected statistical and systematic uncertainties of the new experiments. The total point-to-point uncorrelated uncertainty on the twist-4 term for the Bjorken sum,  $f_2^{p-n}$ , decreases by a factor of 5-6 compared to results obtained in Ref. [61].

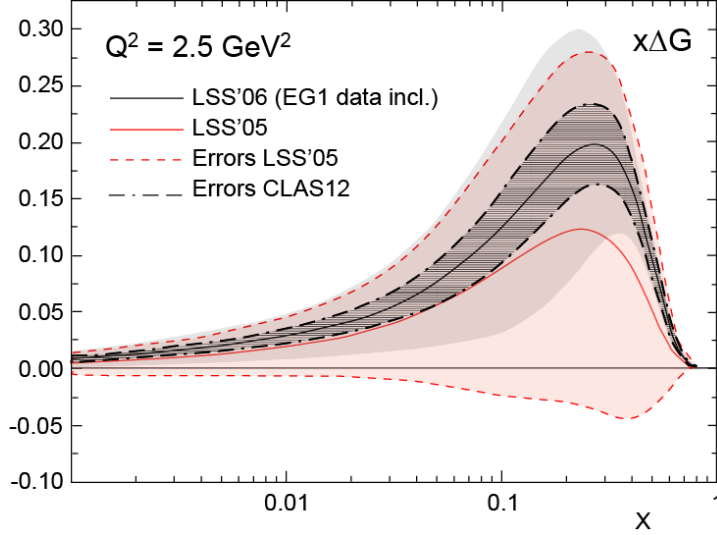


Fig. 15. – Expected uncertainties for  $x\Delta G$ . The black solid curve shows the central value of the present analysis that includes CLAS EG1 data. The dashed-dotted lines give the error band when the expected CLAS12 data are included in the LSS QCD analysis.

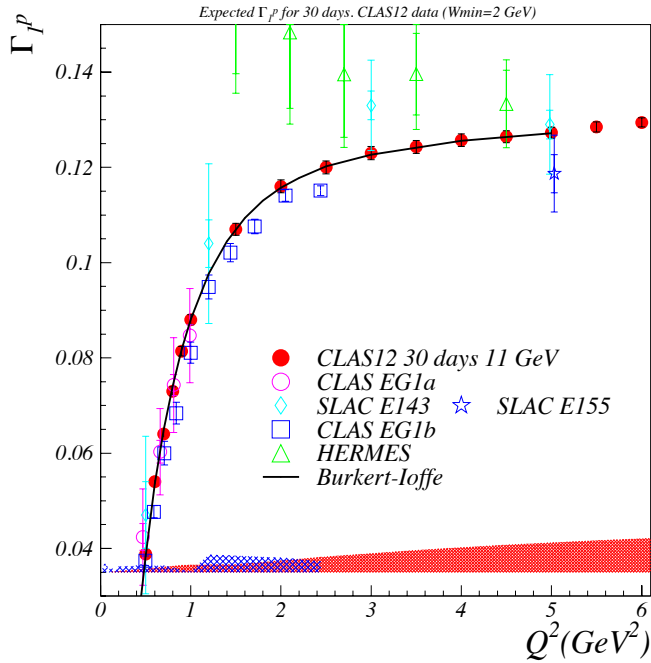


Fig. 16. – Expected precision on  $\Gamma_1^p$  for CLAS12 and 30 days of running. CLAS EG1a [47, 48] data and preliminary results from EG1b are shown for comparison. The data and systematic uncertainties include estimates of the unmeasured DIS contribution. HERMES [55] data, and E143 [56] and E155 data [57] from SLAC are also shown (including DIS contribution estimates). The solid line is a model from [58, 59].

## 6. – Elastic and resonance transition electromagnetic form factors at short distances

**6.1. Nucleon elastic form factors.** – The most basic observables that reflect the composite nature of the nucleon are its electromagnetic form factors. The electric and magnetic form factors characterize the distributions of charge and magnetization in the nucleon as a function of the spatial resolving power. Further, these quantities can be described and related to other observables through the generalized parton distributions discussed in section 3.

Measurements of the elastic form factors continues will remain an important aspect of the physics program at 12 GeV, and will be part of the program in several experiments at JLab [62, 63, 64, 65, 66]. The magnetic form factor of the neutron requires special experimental setups for neutron detection and the in-situ neutron efficiency calibration measurement, for which CLAS12 is well suited. Figure 17 shows the existing data as well as the extension in  $Q^2$  projected for the 12 GeV program.

Nucleon ground and excited states represent different eigenstates of the Hamiltonian, therefore to understand the interactions underlying nucleon formation from fundamental constituents, the structure of both the ground state and the excited states must be studied.

**6.2. Nucleon resonance transition form factors.** – The nucleon resonance transition form factors reveal the nature of the excited states and encode the transition charge and current densities on the light cone. The  $N^*$  program at JLab (for recent overviews see: [67, 68]) has already generated results for the transition form factors at  $Q^2$  up to 6 GeV<sup>2</sup> for the  $\Delta(1232)$ , and up to 7.5 GeV<sup>2</sup> for the  $N(1535)S_{11}$ . The latest results [69, 70] on the transition form factors of the Roper resonance  $N(1440)P_{11}$  for  $Q^2$  up to 4.5 GeV<sup>2</sup>, have demonstrated the sensitivity to the degrees of freedom that are effective in the excitation of particular states. The JLab energy upgrade will allow us to probe resonance excitations at much higher  $Q^2$  [71], where the elementary quarks degrees of freedom may become evident in the resonance formation through the approach to scaling as constituents quarks are stripped of the gluon cloud and approach their asymptotic mass values. Resonance transition form factors are sensitive to the effective quark mass. Figure 18 shows the projected  $Q^2$  dependence of the  $A_{1/2}$  transition amplitude for the  $N(1440)P_{11}$  resonance obtained from single pion production. Resonances at higher mass tend to decouple from the single pion channel. The transition form factors of those excited states can be efficiently measured in double-pion processes [72] such as  $ep \rightarrow ep\pi^+\pi^-$ .

## 7. – Gluonic Hadron spectroscopy.

The presence of gluons has been established in high energy  $e^+e^-$  collisions where the reaction  $e^+e^- \rightarrow 3$  jets was observed. This process is predicted in perturbative QCD and is quantitatively described as the result of hard gluon bremsstrahlung from one of the high energy quarks in the annihilation process  $e^+ + e^- \rightarrow q + \bar{q} + g$ . One of the open problems in hadron physics is if gluons (or the "glue") actively participate processes at low energy, such as the excitations of hadrons. The most promising way of establishing the effect of the "glue" in spectroscopy is the study of the meson spectrum.

**7.1. Hybrid mesons.** – Our understanding of how quarks form mesons has evolved within QCD and we expect a rich spectrum of mesons that takes into account not only the quark degrees of freedom, but also the gluonic degrees of freedom. Excitations of the gluonic field binding the quarks can give rise to excitations of the glue (hybrid mesons). A picture of these hybrid mesons is one where these particles are excitations of a gluonic flux tube that forms between the quark and antiquark. Particularly interesting is that many of these hybrid mesons are expected to have exotic quantum numbers  $J^{PC} = 0^{+-}, 1^{-+}, 2^{+-}$  that cannot be achieved in simple  $q\bar{q}$  systems. In the flux tube model these states do not mix with conventional meson states which simplifies dramatically the search for hybrid mesons. The isolation of mesons with exotic quantum numbers provides strong evidence for gluonic excitations, however they do not uniquely identify hybrid mesons. Other complex configurations, such as 4-quark states ( $qq\bar{q}\bar{q}$ )

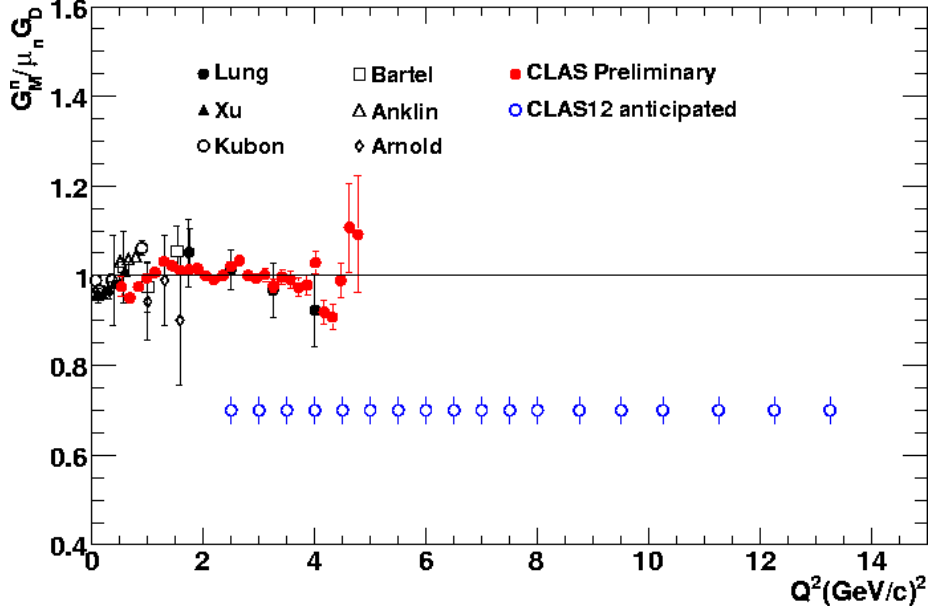


Fig. 17. – The magnetic form factor for the neutron. The existing data, and projected uncertainties at 12 GeV with CLAS12 (blue open circles).

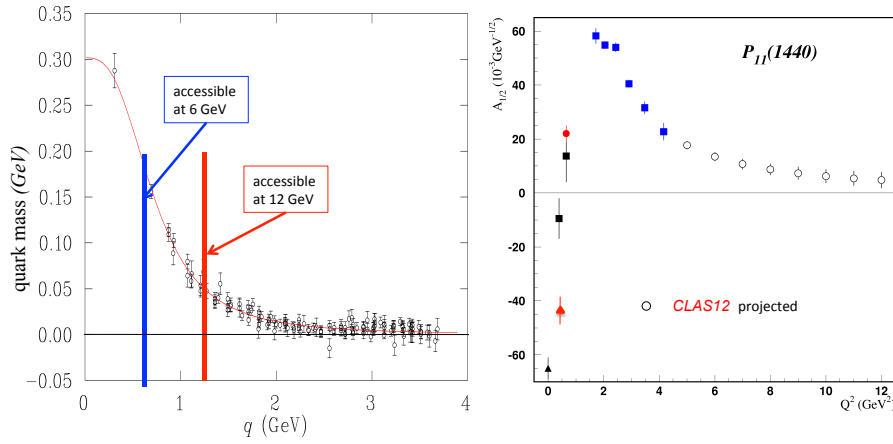


Fig. 18. – Left panel: Evolution of the quark mass with momentum transfer. The region left of the blue line is accessible at 6 GeV beam energy, the region left of the red line can be accessed at 12 GeV in  $N^*$  excitations with  $Q^2 \leq 12 \text{ GeV}^2$ . Right panel: Published and projected electro-coupling amplitudes for the Roper resonance with a 12 GeV electron beam.

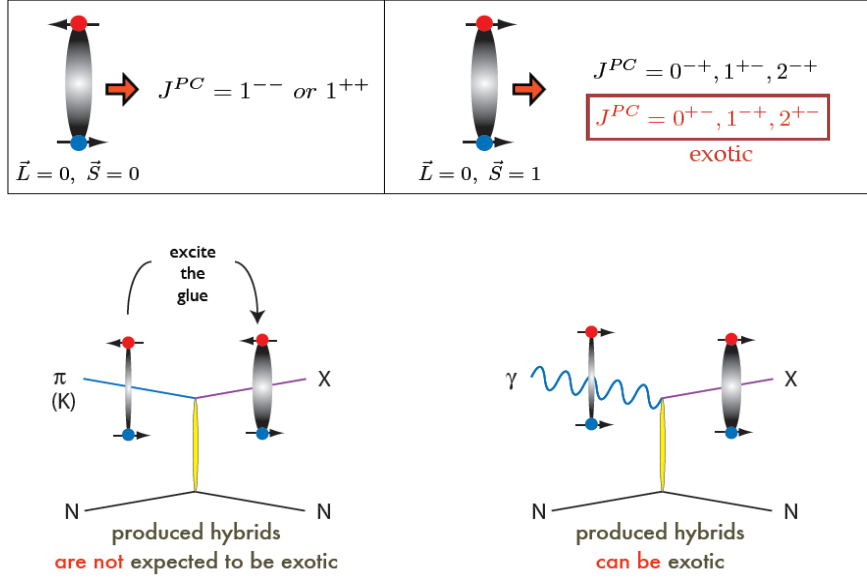


Fig. 19. – Possible production mechanisms of mesons with exotic quantum numbers with photon beams. In this picture mesons with exotic quantum numbers are preferentially produced in reactions with real photons.

may also have same quantum numbers. For that reason it is essential to establish not only the existence of one or two states, but as many states as possible to characterize the systematics of the spectrum. The level splitting between the ground state flux tube and the first excited transverse modes is expected to be about  $1 \text{ GeV}/c^2$ , and lattice QCD calculations indicate the lightest exotic hybrid (the  $J^{PC} = 1^{-+}$ ) has a mass of about  $1.9 \pm 0.2 \text{ GeV}$ .

There are tantalizing suggestions, mainly from experiments using beams of  $\pi$  mesons, that exotic hybrid mesons do exist. The evidence is by no means clear cut, owing in part, to the apparently small production rates for these states in the decay channels examined. It is safe to conclude that the extensive data collected to date with probes have not uncovered the hybrid meson spectrum. Based on models, such as the flux-tube model, we expect the production of hybrid mesons in photon induced reactions to be comparable to the production of normal mesons. Photoproduction of mesons using a  $\approx 9 \text{ GeV}$ , linearly polarized photon beam provides a unique opportunity to search for exotic hybrids. Existing data are extremely limited for charged final states, and no data exist for multi-neutral final states. To carry out such a search, the GlueX [73] program in Hall D will look at many different final states involving both charged particles and photons, but particular emphasis will be placed on those reactions that have 3 or more pions in the final state. The discovery potential for GlueX comes first from the very high statistics based on  $10^7$  tagged photons per second on target, which will exceed existing photoproduction data by several orders of magnitude. The GlueX experimental search in Hall

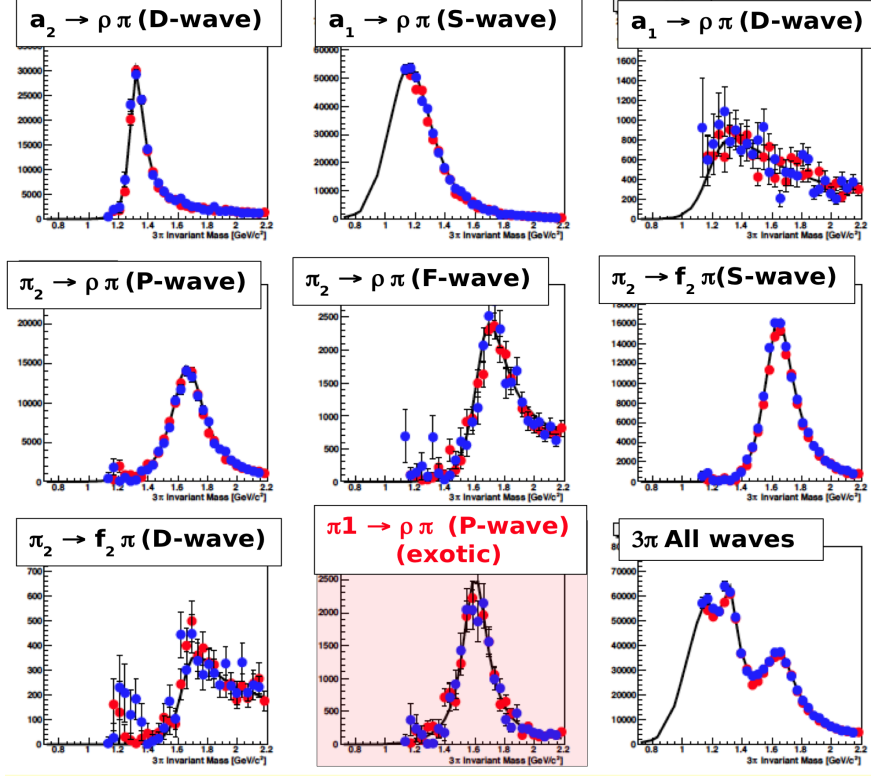


Fig. 20. – Events with 3-pions in the final state are generated in specific partial waves (solid lines) including one with exotic  $J^{PC}$  quantum numbers, and then tracked through the CLAS12 detector system and then reconstructed (points with error bars). They reconstructed events retain their initial partial wave contents.

D has a mass reach up to about 2.8 GeV to observe mesons with masses up to 2.5 GeV/c<sup>2</sup>.

An alternative approach has been taken in Hall B with CLAS12, which uses a quasi-real photon beam energy-tagged at very forward electron scattering angles. The Forward Tagger (FT) makes use of a high granularity, high resolution crystal calorimeter to detect the small angle electrons in the energy range of up to 4 GeV [74]. The difference to photon energy tagging of real photons is that it allows running the experiment at a much higher effective luminosity than is possible when tagging real photons. The reason is that real photon tagging requires two independent interactions - the real photon being generated in an electromagnetic interaction with the atomic electrons of the radiator by bremsstrahlung, and the real photon interacting hadronically with the proton in the production target. The latter process has a typical probability of about 1% only. In virtual photon tagging the photon interacts hadronically in the production target, potentially allowing much higher production rates to be achieved in experiments compared to real photo-production. Another aspect is that virtual photons are linearly polarized providing an important degree of freedom that can be utilized in the partial

wave analysis of multi-particle final states to reduce ambiguities. Figure 20 shows the results of a partial wave analysis. The events are simulated with different partial wave content, then tracked through the CLAS12 acceptance and then subjected to a partial wave analysis. The results of the analysis show that the initial partial wave content is preserved.

**7.2. Hybrid baryons.** – The search for gluonic excitations has so far be limited to mesons, however baryons may also be excited through the their gluon degrees of freedom. Studies of hybrid baryons are equally important to hybrid mesons in the quest to better understand the complex confinement mechanisms in hadrons. However, gluonic baryons  $|qqqG\rangle$  and ordinary 3-quark baryons  $|qqq\rangle$  have the same quantum number, making it impossible to uniquely separate them from each other. One possibility is to distinguish different types of baryons due to a possible overpopulation of states with specific spin-parity  $J^P$  assignments in comparison

TABLE III. – *Expected hadron production rates for 1,000 DIS events at 11GeV beam energy.*

hadron	$c\tau$	mass (GeV)	flavor content	detection channel	Production rate per 1k DIS events
$\pi^0$	25 nm	0.13	$u\bar{u}d\bar{d}$	$\gamma\gamma$	1100
$\pi^+$	7.8 m	0.14	$u\bar{d}$	direct	1000
$\pi^-$	7.8 m	0.14	$d\bar{u}$	direct	1000
$\eta$	0.17 nm	0.55	$u\bar{u}d\bar{d}s\bar{s}$	$\gamma\gamma$	120
$\omega$	23 fm	0.78	$u\bar{u}d\bar{d}s\bar{s}$	$\pi^+\pi^-\pi^0$	170
$\eta'$	0.98 pm	0.96	$u\bar{u}d\bar{d}s\bar{s}$	$\pi^+\pi^-\eta$	27
$\phi$	44 fm	1.0	$u\bar{u}d\bar{d}s\bar{s}$	$K^+K^-$	0.8
$f_1$	8 fm	1.3	$u\bar{u}d\bar{d}s\bar{s}$	$\pi\pi\pi\pi$	-
$K^+$	3.7 m	0.49	$u\bar{s}$	direct	75
$K^-$	3.7 m	0.49	$\bar{u}s$	direct	25
$K^0$	27 mm	0.50	$d\bar{s}$	$\pi^+\pi^-$	42
$p$	stable	0.94	$ud$	direct	530
$\bar{p}$	stable	0.94	$\bar{u}\bar{d}$	direct	3
$\Lambda$	79 mm	1.1	$uds$	$p\pi^-$	72
$\Lambda(1520)$	13 fm	1.5	$uds$	$p\pi^-$	-
$\Sigma^+$	24 mm	1.2	$us$	$p\pi^0$	6
$\Sigma^0$	22 pm	1.2	$uds$	$\Lambda\gamma$	11
$\Xi^0$	87 mm	1.3	$us$	$\Lambda\pi^0$	0.6
$\Xi^-$	49 mm	1.3	$ds$	$\Lambda\pi^-$	0.9

to the number of such states that are predicted in the constituent quark model. The excited glue adds  $\approx 1$  GeV to the mass of hybrid baryons, putting the lowest mass hybrid baryons with strangeness  $S = 0$  into the range from 1.8 to 2 GeV.

## 8. – Quarks and hadrons in the nuclear medium

**8.1. Color Transparency.** – Color transparency (CT) is a unique prediction of QCD, and implies that under certain conditions, the nuclear medium will allow the transmission of hadrons with reduced absorption. The phenomenon of CT is predicted on the quark-gluon basis and is totally unexpected on a hadronic interaction picture. The following conditions must be present to observe CT: the interactions must create a small size object (point-like configuration, PLC) that has a small cross section when traveling in a hadronic medium, and the distance over which it expands to its full hadronic size must be larger than the nucleus size. Such conditions require high enough energy transfer to the target where the photon couples to PLCs, and the full hadronization occurs outside the nucleus. Color transparency effects have been observed at very high energies at hadron machines, but at what momentum transfer CT sets in is still a not fully settled question. Small increases in nuclear transparency consistent with theoretical predictions have been observed at JLab with 5-6 GeV electron beams in pion production. The energy doubling of the JLab electron accelerator to 12 GeV will provide much better conditions where a significantly increased transparency should be observable [75, 76] with high sensitivity, as is shown, e.g. in Fig. 21.

**8.2. Quark propagation and hadron formation..** – The use of electron beams at 12 GeV allows us to address fundamental questions of how colored quarks struck in the interaction with high energy photons transform into colorless hadrons. Questions that we want to have answered are, how long can a light colored quark remain de-confined? The production time  $T_p$  measured this quantity. Because de-confined quarks emit gluons,  $T_p$  can be measured via medium-stimulated gluon emission resulting in a broadening of the transverse momentum distribution of the final hadrons. Another important question to address is: How long does it take to form the color field of a hadron? This can be measured by the formation time  $T_f^h$ . Since hadrons interact strongly with the nuclear medium,  $T_f^h$  can be determined by measuring the attenuation of hadrons in the nuclear medium by using nuclei of different sizes.

These question can be addressed by measuring the hadronic multiplicity ratio

$$R_M^h(z, \nu, p_T^2, Q^2, \phi) = \frac{\left\{ \frac{N_h^{DIS}(z, \nu, p_T^2, Q^2, \phi)}{N_e^{DIS}(\nu, Q^2)} \right\}_A}{\left\{ \frac{N_h^{DIS}(z, \nu, p_T^2, Q^2, \phi)}{N_e^{DIS}(\nu, Q^2)} \right\}_D}$$

versus all kinematical quantities. In this expression,  $N_h$  is the number of hadrons produced in DIS events and  $N_e^{DIS}$  is the number of associated DIS electrons. The numerator corresponds to target nucleus  $A$ , and the denominator corresponds to deuterium.  $\nu$  is the energy transferred by the electron, and  $z$  is the hadron energy divided by  $\nu$ . In the QCD-improved parton model,  $R_M^h$  is given by the ratios of sums over products of the quark distribution functions with fragmentation functions. This measurement [77] will provide two to three orders of magnitude more data than any previous experiment in this energy range and will include a much larger collection of hadron species. Table III shows the expected rates for the production of a large number of hadron species. Examples of projected data for the multiplicity ratio  $R_M^h(z, \nu, p_T^2, Q^2, \phi)$  are shown in Fig. 22.

## 9. – Search for new Physics

**9.1. Search for deviations from the Standard Model.** – The Standard Model (SM) of High Energy Physics has been highly successful in accurately predicting a large number of experimental observations. Its predictions have been probed at the highest energy accelerators at HERA, the Tevatron at Fermilab, and now at the LHC at CERN. So far, no clear deviations from

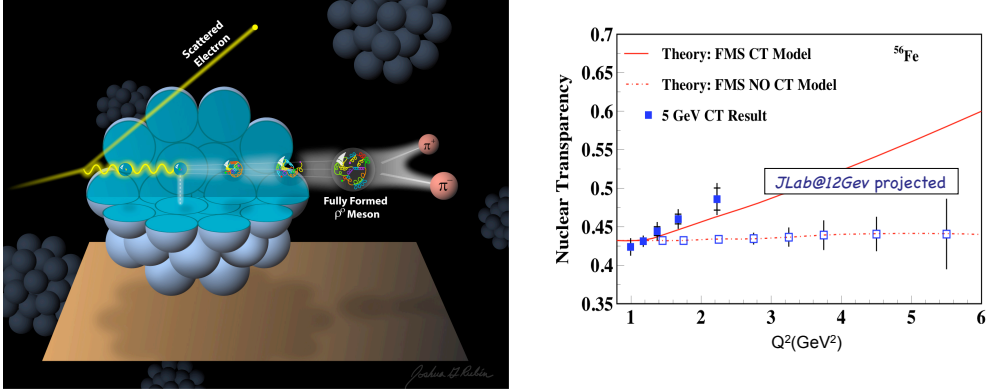


Fig. 21. – Projected color transparency effects in Fe. The open circles represent projected results with CLAS12 at 12 GeV.

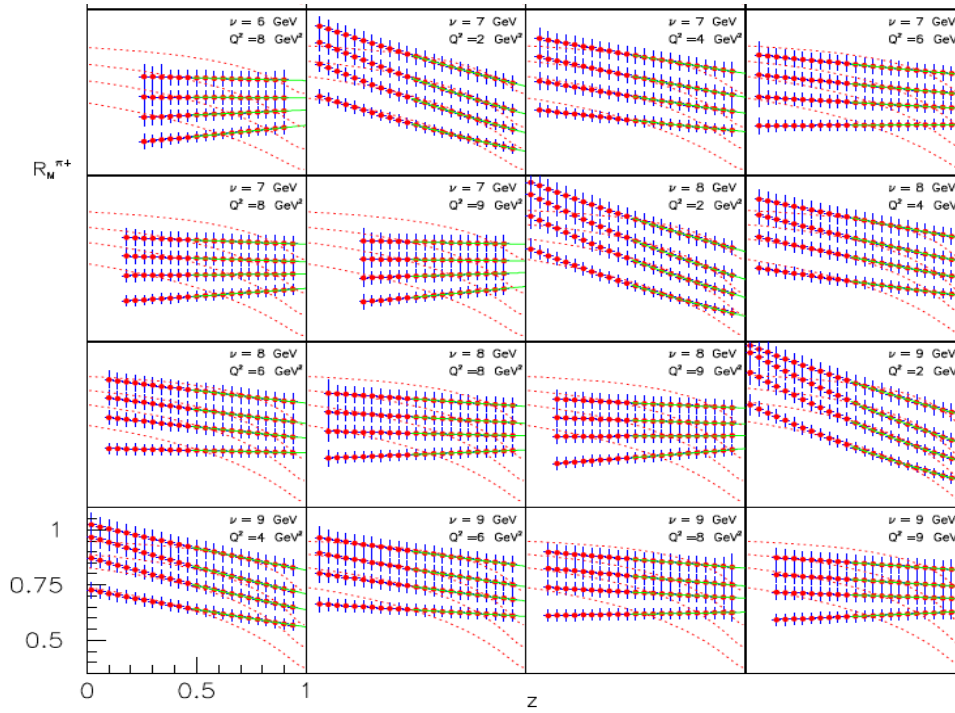


Fig. 22. – Z dependence of the hadronic multiplicity ratio (top to bottom in each plot) for  $^{14}\text{N}$ ,  $^{40}\text{Ar}$ ,  $^{197}\text{Au}$  for 16 bins in  $Q^2$ ,  $\nu$ . The solid line is a gluon bremsstrahlung model calculation [?] for  $z > 0.5$  for pions. The dotted lines are parameterizations of HERMES 27 GeV data.

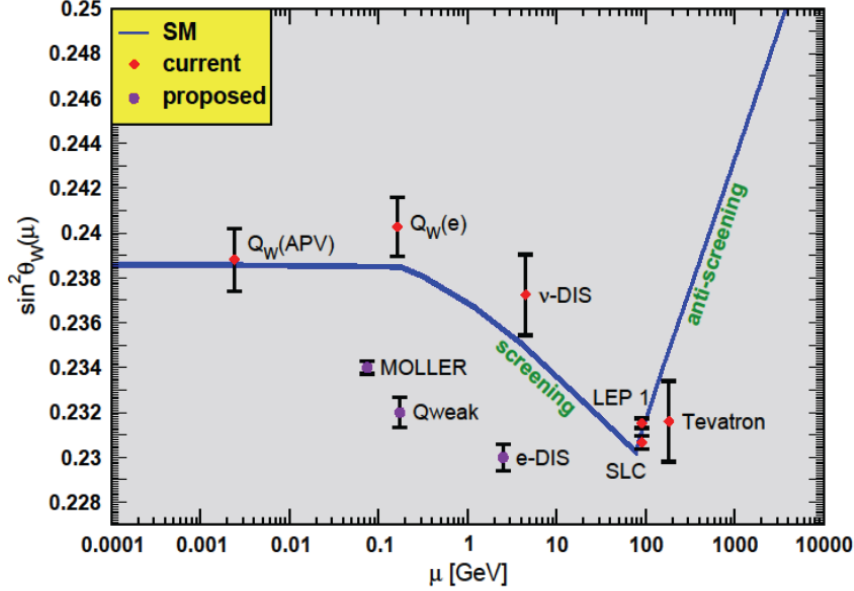


Fig. 23. – Current knowledge of the weak mixing angle in comparison to the SM predictions .

the SM have been identified. While most of the searches for physics beyond the SM involve very high-energy accelerators where new particle types may be produced in high-energy collisions, deviations from the SM may also be observed in high precision experiments at lower energies. Parity violating electron scattering may be the best tool to study possible SM violating effects in precision measurements of the electro-quark couplings that relate to the weak mixing angle  $\sin^2 \Theta_W$ . New physics such as quark compositeness, or new gauge bosons beyond the  $Z^0$ , may cause small deviations from the SM predictions at relatively low energies that can be revealed in very high precision experiments. With the high luminosity available at JLab such effects may be detectable. Two experiments have been proposed to measure with high precision the weak mixing angle  $\sin^2 \Theta_W$  in parity violating electron-electron scattering (Moller scattering) [78], and in deep inelastic electron scattering [79]. Figure 23 shows the Standard Model prediction for the energy dependence of the weak mixing angle in comparison with measurements. Previous measurements indicate a possible discrepancy for several of the data points each one at the  $\geq 1\sigma$  level. The new measurements will significantly improve the precision of the experimental data base.

**9.2. Heavy photon search.** – Recent satellite measurements have shown a dramatic excess of positrons ranging in energy from 10GeV to several hundred 100GeV. One interpretation for this anomaly is the existence of a new gauge vector boson that couples very weakly to  $e^+e^-$  pairs and can be produced through interaction with the dark matter in the universe, see Fig. 24. New light vector particles and their associated interactions are ubiquitous in extensions of the Standard Model. However, the symmetries of the Standard Model restrict the interaction of ordinary matter with such new states. Indeed, most interactions consistent with Standard Model gauge symmetries and Lorentz invariance have couplings suppressed by a high mass scale. One of the few unsuppressed interactions is the coupling of charged Standard Model particles to a

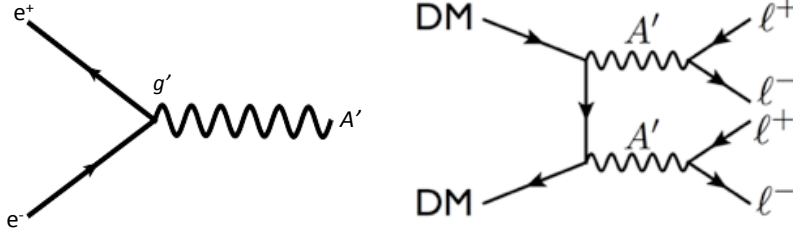


Fig. 24. – Possible graphs contributing to the excess of positrons (left) and the coupling of the purported  $A'$  vector-boson to dark matter (right).

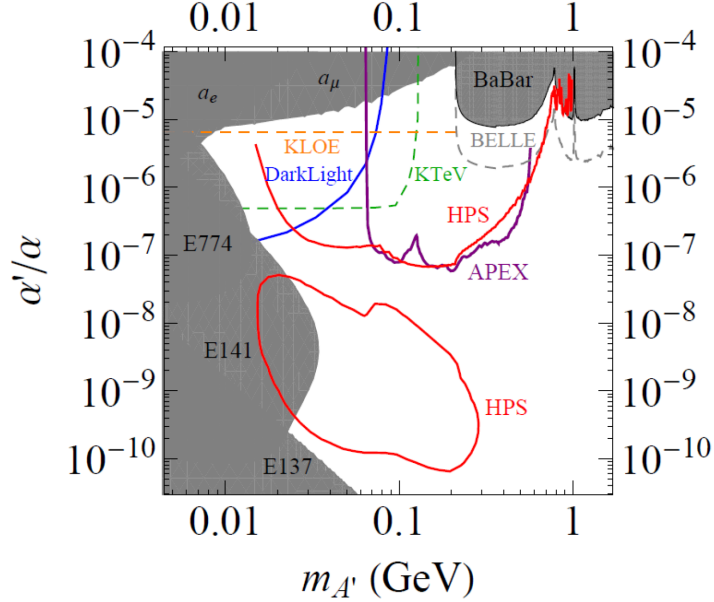


Fig. 25. – Exclusion zones for the ratio of heavy photon to electromagnetic coupling strengths to  $e^+e^-$  pairs versus the heavy photon mass. The various lines show the exclusion zones from previous and planned measurements. The proposed and planned measurements at JLab are shown by the lines marked HPS and APEX. The two zones in the upper part are for the HPS and APEX experiment to search for narrow peaks in the mass spectrum of the  $e^+e^-$  pair. The zone marked HPS in the lower part includes the search for detached vertices that would indicate the presence of a long-lived  $A'$  with weak coupling.

new gauge boson  $A'$ , which is quite poorly constrained for small coupling constants as shown in Fig. 25.

Heavy photons mix with the ordinary photon through kinetic mixing, which induces their

weak coupling to electrons,  $\epsilon e$ , where  $\epsilon \approx 10^{-3}$ . Since they couple to electrons, heavy photons are radiated in electron scattering and can subsequently decay into narrow  $e^+e^-$  resonances which can be observed above the copious QED trident background. For suitably small couplings, heavy photons travel detectable distances before decaying, providing a second signature. Two experiments have been proposed at JLab [80, 81] to extend considerably the kinematic zone covered by experiment in the search for a new gauge boson. The APEX experiment in Hall A [80] uses high resolution magnetic spectrometers to search for narrow peaks in the  $e^+e^-$  mass spectrum. The HPS experiment in Hall B, in addition to searching for peaks in the mass spectrum also searches for detached vertices from the decay of a long-lived  $A'$ . The latter probes a region with much weaker coupling of the  $A'$  to  $e^+e^-$  pairs as seen in the bottom part of Fig. 25.

## 10. – Conclusions

The JLab energy upgrade and the planned new experimental equipment are well matched to an exciting scientific program aimed at studies of the complex nucleon structure in terms of the newly discovered longitudinal and transverse momentum dependent parton distribution functions, the GPDs and TMDs. They provide fundamentally new insights in the complex multi-dimensional quark structure of the nucleon. The exploration of the gluonic meson excitations is a complementary effort to study the active role of gluons play in the excitation spectrum of hadrons. In addition, the high precision afforded by the high luminosity and the large acceptance detectors, and the development of novel techniques to measure scattering off nearly free neutrons, will enable the exploration of phase space domains with extreme conditions that could not be studied before.

\* \* \*

I like to thank my colleagues at Jefferson Lab for many discussions on the exciting science with the JLab 12GeV upgrade and for providing me with many of the graphs that I included in this contribution. This work was carried out under DOE contract No. DE-AC05-06OR23177.

## REFERENCES

- [1] MUELLER D. ET AL., *Fortsch. Phys.*, **42** (1994) 101, hep-ph/9812448.
- [2] JI X., , *Phys. Rev. D*, **55** (1997) 7114.
- [3] JI X. ,*Phys. Rev. Lett.*, **8** (1997) 610.
- [4] RADYUSHKIN A.,*Phys. Lett. B*, **380** (1996) 417.
- [5] RADYUSHKIN A., *Phys. Rev. D*, **56** (1997) 5524.
- [6] BELITSKY A.V., MUELLER D., KIRCHNER A., Nucl. Phys. B6292002 323.
- [7] BURKARDT M, *Int. J. Mod. Phys. A*, **18** (2003) 173.
- [8] BELITSKY A.V., JI X., YUAN F.,*Phys. Rev. D*, **69** (2004) 074014.
- [9] GOEKE K. ET AL., *Phys. Rev. D*, **75** (2007) 094021.
- [10] STEPANYAN S. ET AL., *Phys. Rev. Lett.*, **87** (2001) 182002.
- [11] GIROD F.X. ET AL., *Phys. Rev. Lett.*, **100** (2008) 162002.
- [12] MUNOZ-CAMACHO C. ET AL.,*Phys. Rev. Lett.*, **97** (2006) 262002.
- [13] CHEN S. ET AL., *Phys. Rev. Lett.*, **97** (2006) 072002.
- [14] A. Airapetian, et al., *Phys. Rev. Lett.* **87**, 182001, 2001.
- [15] JLAB EXPERIMENT E12-06-119, SABATIE F. ET AL.,(2006).
- [16] JLAB LETTER OF INTENT LOI11-105, ELOUADRHIRI L. ET AL.,(2011).
- [17] DE MASI R. ET AL.,*Phys. Rev. C*, **77** (2008) 042201.
- [18] JLAB EXPERIMENT E12-10-114, HYDE C. ET AL., (2010).
- [19] JLAB EXPERIMENT E12-11-003, NICCOLAI S. ET AL.,(2011).
- [20] VANDERHAEGHEN M., GUICHON M., GUIDAL M., *Phys. Rev. D*, **60** (1999) 094017.
- [21] SIVERS W.D., *Phys.Rev.D*, **4** (1990) 83.
- [22] BOER D. and MULDER P.J., *Phys. Rev. D*, **57** (1998) 5780.
- [23] MULDER P.J. and TANGERMAN R.D., *Nucl. Phys. B*, **461** (1996) 197.

- [24] JLAB EXPERIMENT E12-09-017, ENT R. ET AL.,(2009).
- [25] JLAB EXPERIMENT E12-09-007, AVAKIAN H. ET AL.,(2009).
- [26] JLAB EXPERIMENT E12-09-008, AVAKIAN H. ET AL.,(2009).
- [27] JLAB EXPERIMENT E12-06-112, AVAKIAN H. ET AL.,(2006).
- [28] JLAB EXPERIMENT E12-09-018, WOJTSEKOWSKI B. ET AL.,(2009).
- [29] JLAB EXPERIMENT E12-07-107, AVAKIAN H. ET AL.,(2007).
- [30] JLAB EXPERIMENT E12-09-009, AVAKIAN H. ET AL.,(2009).
- [31] JLAB EXPERIMENT E12-11-007, HUANG J. ET AL., (2011)
- [32] JLAB EXPERIMENT C12-11-111, CONTALBRIGO M. ET AL.,(2011).
- [33] JLAB EXPERIMENT E12-11-006, GAO H. ET AL.,(2011).
- [34] JLAB EXPERIMENT E12-11-111, CONTALBRIGO M. ET AL.,(2011).
- [35] JLAB EXPERIMENT E12-11-108, GAO H. ET AL.,(2011).
- [36] ZHENG X. ET AL., *Phys. Rev. C*, **70** (2004) 065207.
- [37] BOSTED P. ET AL., *Phys. Rev. C*, **75** (2007) 035203.
- [38] BAILLIE N. ET AL, arXiv:1110.2770(2011).
- [39] CHRISTY M.E. and MELNITCHOUK W., *J. Phys.: Conf. Ser.*, **299** (2011) 01200
- [40] CHEN J.P., DEUR A., KUHN S., MEZIANI Z.E., *J. Phys.: Conf. Ser.*, **299** (2011) 012005
- [41] JLAB EXPERIMENT E12-10-113, BUELTMAN S. ET AL., (2010).
- [42] JLAB EXPERIMENT E12-10-103, PETRATOS G. ET AL., (2010).
- [43] JLAB EXPERIMENT E12-06-109, KUHN S. ET AL.,(2006)
- [44] JLAB EXPERIMENT E12-06-110, MEZIANI Z.E. ET AL., (2006).
- [45] JLAB EXPERIMENT E12-06-122, CATES G. ET AL., (2006).
- [46] LEADER E.,SIDOROV S.,and STAMENOV D., *Phys. Rev. D*, **75** (2007) 074027.
- [47] FATEMI R. ET AL., *Phys. Rev. Lett.*, **91** (2003) 222002.
- [48] YUN J. ET AL., *Phys. Rev. C*, **67** (2003) 055204.
- [49] AMARIAN M. ET AL.,*Phys. Rev. Lett.* , **92** (2004) 022301.
- [50] PROK Y. ET AL.,*Phys.Lett. B*, **672** (2009) 12.
- [51] DHARMAWARDANE V. ET AL., *Phys. Lett. B*, **641** (2006) 11.
- [52] BJORKEN J.D., *Phys. Rev.* , **148** (1966) 1467.
- [53] THOMAS E. and BIANCHI N., *Nucl. Phys. Proc. Suppl.*, **82** (2000) 26.
- [54] OSIPENKO M. ET AL., *PHYS. REV. D*,712005054007.
- [55] AIRAPETIAN A. ET AL., *Eur. Phys. J. C*, **26** (2003) 527.
- [56] ABE K. ET AL., *Phys. Rev. D*, **58** (1998) 112003.
- [57] ANTHONY P.L. ET AL.,*Phys. Lett. B*, **493** (2000) 19.
- [58] BURKERT V.D. and IOFFE B.L., *Phys. Lett. B*, **296** (1992) 223.
- [59] BURKERT V.D. and IOFFE B.L.,*J. Exp. Theor. Phys.*, **78** (1994) 619
- [60] CHEN J.P., DEUR A., MEZIANI Z.-E., *Mod. Phys. Lett. A*, **20** (2005) 2745.
- [61] DEUR A. ET AL., *Phys. Rev. Lett.*, **93** (2004) 212001.
- [62] JLAB EXPERIMENT E12-07-104, GILFOYLE G. ET AL., (2007).
- [63] JLAB EXPERIMENT E12-07-109, BRASH E. ET AL., (2007).
- [64] JLAB EXPERIMENT E12-09-019, WOJSTEKHOWSKI B. ET AL., (2009).
- [65] JLAB EXPERIMENT E12-09-016, WOJSTEKHOWSKI B. ET AL., (2009).
- [66] JLAB EXPERIMENT E12-11-105, MOFFIT B. ET AL., (2007).
- [67] AZNAURYAN I. G. and BURKERT V.D., *Prog.Part.Nucl.Phys*, **67** (2012) 1-54
- [68] AZNAURYAN I.G., BURKERT V.D., LEE T.-S.H., MOKEEV V., *J.Phys.Conf.Ser.*, **299** (2011) 012008
- [69] AZNAURYAN I. ET AL.,*Phys. Rev. C*, **78** (2008) 045209.
- [70] AZNAURYAN I. ET AL.,*Phys. Rev. C*, **80** (2009) 055203.
- [71] JLAB EXPERIMENT E12-09-103, GOTHE R., MOKEEV V., ET AL., (2009).
- [72] RIPANI M. ET AL., *Phys. Rev. Lett.*, **91** (2003) 022002.
- [73] JLAB EXPERIMENT E12-06-102, MEYER C. ET AL., (2006).
- [74] JLAB EXPERIMENT E12-11-105, BATTAGLIERI M. ET AL., (2011).
- [75] JLAB EXPERIMENT E12-06-106, HAFIDI K. ET AL., (2006).
- [76] JLAB EXPERIMENT E12-06-107, DUTTA D. ET AL., (2006).
- [77] JLAB EXPERIMENT E12-06-117, BROOKS W. ET AL., (2006).

- [78] JLAB EXPERIMENT E12-09-005, KUMAR K. AT AL., (2009).
- [79] JLAB EXPERIMENT E12-10-007, SOUNDER P. ET AL., (2010).
- [80] JLAB EXPERIMENT E12-10-009, SCHUSTER P., ET AL., (2010).
- [81] JLAB EXPERIMENT C12-11-006, JAROS J. ET AL.,(2011).